Available online at www.sciencedirect.com
ScienceDirect
Biochimica et Biophysica Acta 1758 (2006) 923–933
BIOCHIMICA ET BIOPHYSICA ACTA
BBA
www.elsevier.com/locate/bbamem

Review

Determination of molecular conformation and permeation in skin via IR spectroscopy, microscopy, and imaging

Richard Mendelsohn [a,*], Carol R. Flach [a], David J. Moore [b]

[a] *Department of Chemistry, Newark College, Rutgers University, 73 Warren Street, Newark, NJ 07102, USA*
[b] *International Specialty Products, 1361 Alps Road, Wayne, NJ 07470, USA*

Received 20 January 2006; received in revised form 17 February 2006; accepted 11 April 2006
Available online 21 April 2006

Abstract

Skin tissue, in addition to its specific use in dermal research, provides an excellent model for developing the techniques of vibrational microscopy and imaging for biomedical applications. In addition to permitting characterization of various regions of skin, the relative paucity of major biological constituents in the stratum corneum (the outermost layer of skin), permits us to *image*, with microscopic resolution, conformational alterations and concentration variations in both the lipid and protein components. Thus we are able to monitor the effects of exogenous materials such as models for drug delivery agents (liposomes) and permeation enhancers (DMSO) on stratum corneum lipid organization and protein structure. In addition, we are able to monitor protein conformational changes in single corneocytes. The current article demonstrates these procedures, ranging from direct univariate measures of lipid chain conformational disorder, to factor analysis which permits us to image conformational differences between liposomes that have permeated through the stratum corneum from those which have remained on the surface in a reservoir outside the skin.

Keywords: Stratum corneum; IR microscopy and imaging; Lipid phase behavior; Liposome permeation

Contents

* Corresponding author.
E-mail address: mendelso@andromeda.rutgers.edu (R. Mendelsohn).

0005-2736/$ - see front matter © 2006 Elsevier B.V. All rights reserved.
doi:10.1016/j.bbamem.2006.04.009

1. Introduction

The burgeoning technologies of IR and Raman microscopy and spectroscopic imaging provide spatially resolved molecular information from tissues, and will permit applications ranging from the diagnosis of disease states in biopsies, to studies of the effects of therapeutic intervention, to identification of exogenous substances. Initial missteps using traditional (non-spatially resolved) IR for the diagnosis of cancer have been rectified and IR imaging is progressing, with demonstrable success, to become a reliable addition to traditional methods of pathology.

A considerable advantage of vibrational microscopy and imaging, somewhat overlooked in biomedical applications, is direct access to molecular structure information. For example, unlike confocal fluorescence microscopy, where the image obtained is that of the fluorophore, IR microscopy provides a complete IR spectrum from each illuminated pixel. Thus, the well-established sensitivity of the vibrational spectrum to molecular conformation is retained and becomes accessible in a spatially resolved manner. Normally, in complex preparations such as biopsies used for diagnosis, the number and heterogeneous spatial distribution of constituents renders it difficult to extract information concerning the molecular structure of a particular molecular component or class.

Due to the relatively small number of major constituents in skin and bone, these tissues provide the opportunity not only to use the power of multivariate statistics for diagnostic purposes but also to provide structural information. The confluence of these two aspects of vibrational microscopy and imaging offers the possibility of deducing the molecular structure changes that accompany disease states. Applications along these lines to bone disease are demonstrated elegantly by Professor Adele Boskey and her colleagues elsewhere in this volume. The current article deals with our initial applications of IR microscopy and imaging to skin.

We emphasize our studies of the stratum corneum, the outermost layer of the epidermis, which provides the main permeability barrier and maintains water homeostasis. The organization of this article is as follows: Following a brief recapitulation of some experimental aspects and skin micro-anatomy, conformation-sensitive features of the vibrational spectra of skin lipids are summarized. Next, the type of molecular structure information available from vibrational microscopy and imaging is demonstrated using IR approaches with progressively better spatial resolution starting with transmission measurements from isolated SC (no spatial resolution), ATR from tape-stripped skin (Z resolution of ~0.5 μm), and IR imaging of microtomed skin (X, Y, and Z resolution of ~10 μm). Finally, as a preview of feasible future applications we report initial observations of reversible protein conformational changes in single corneocytes.

2. Experimental considerations

2.1. Sample preparation

The preparation of samples varies significantly from experiment to experiment; all protocols are detailed in our published work [1–5].

2.2. IR imaging

IR microscopic images are acquired with the Perkin Elmer Spotlight system, which consists of an essentially linear array (16×1 detector elements) mercury–cadmium–telluride (MCT) detector along with an automated high precision XY sample stage. Images from specimens (5 μm thick for transmission experiments) may be acquired with rectangular aspect ratios with X, Y dimensions conveniently ranging from 10′s of microns to ~5 mm. A single image may be acquired from 40,000 IR spectra quite conveniently, although more typically, 1/10 to 1/5 of this number are used.

2.3. Data analysis

Spectral Dimensions (Olney, Maryland) ISys 3.0 software was used for analysis and construction of the IR images.

2.4. Spatial resolution and skin structure

The spatial resolution relative to the dimensions of the regions of interest within skin tissue are depicted in Fig. 1 which shows a typical visible micrograph (unstained section) of pigskin. The outermost layer is the stratum corneum (SC).

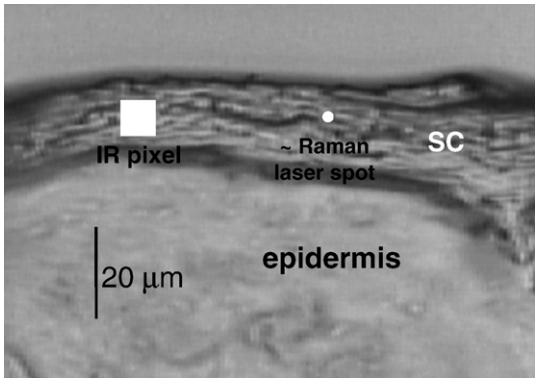

Fig. 1. An optical micrograph of a 10-μm thick unstained pigskin section depicting the stratum corneum (SC) and underlying epidermal regions acquired with a Leica DMLP microscope, a component of the Kaiser Optical Systems Raman Microprobe. The dimensions of an individual pixel in the IR array detector (6.25×6.25 μm) and the approximate laser spot size for Raman sampling (~2 μm) are shown in relation to the size of the skin regions sampled.

Beneath the SC is the viable epidermis. The deepest layer, not depicted in Fig. 1 but shown in Figs. 6A and 7A, is the dermis.

Included in the figure is a white square corresponding to the IR detector pixel size (6.25 × 6.25 μm). The measured, routinely achievable, spatial resolution varies from 10 to 13 μm for methylene stretching modes (wavelength 3.5 μm) and protein Amide I modes (wavelength 6.0 μm), respectively. Also included in the figure is a white circular figure intended to approximate the laser spot size (~2 μm) from which Raman spectra are collected although the current MS deals solely with IR microscopy.

2.5. Background

2.5.1. Skin structure

The functions of the various regions of skin depicted in Figs. 1, 6A and 7A) are considered below:

(i) The SC provides two of the major functions of skin as it (a) forms the main permeability barrier and (b) maintains water homeostasis. Typically, the SC consists of ~10 to 20 cellular layers and is ~10 μm thick when dry, although it may be swelled upon hydration to several times this value. The SC is often viewed as a separate membrane for topical and transdermal drug delivery studies. The SC consists of terminally differentiated, anucleated corneocytes with keratin as the major protein, a cross-linked protein envelope, and an extracellular lamellar lipid network comprised mostly of ceramides, free fatty acids and cholesterol.

(ii) The epidermis, typically 50–150 μm thick, has as one of its primary functions, the generation of the SC. Its principal cell is the keratinocyte, which differentiates as it migrates toward the SC. It takes ~28 days for a daughter keratinocyte from the stratum basale (one of the layers underlying the SC) to terminally differentiate and ultimately shed from the skin's surface.

(iii) The dermis, typically 600–3000 μm thick, is comprised of tough, supportive connective tissue with a variety of specialized structures. Collagen comprises 75% of dry weight of the dermis.

2.5.2. Organization of the SC

The traditional "bricks and mortar" model of macroscopic SC organization is depicted in Fig. 2. In the left hand panel, an AFM view of a polygonal corneocyte (~40 μm in the *X* and *Y* dimensions) isolated from a depth of ~1.5 μm beneath the (human) skin surface is shown. The bottom of this panel depicts the cell thickness, which varies from ~0.5 to 1 μm. The cells are generally elongated.

The lipid matrix in which the cells are embedded is a composite mixture of ceramides, fatty acids and cholesterol. The SC structure depicted in Fig. 2 (central panel) has the lipids ("mortar") surrounding the corneocytes ("bricks"). A

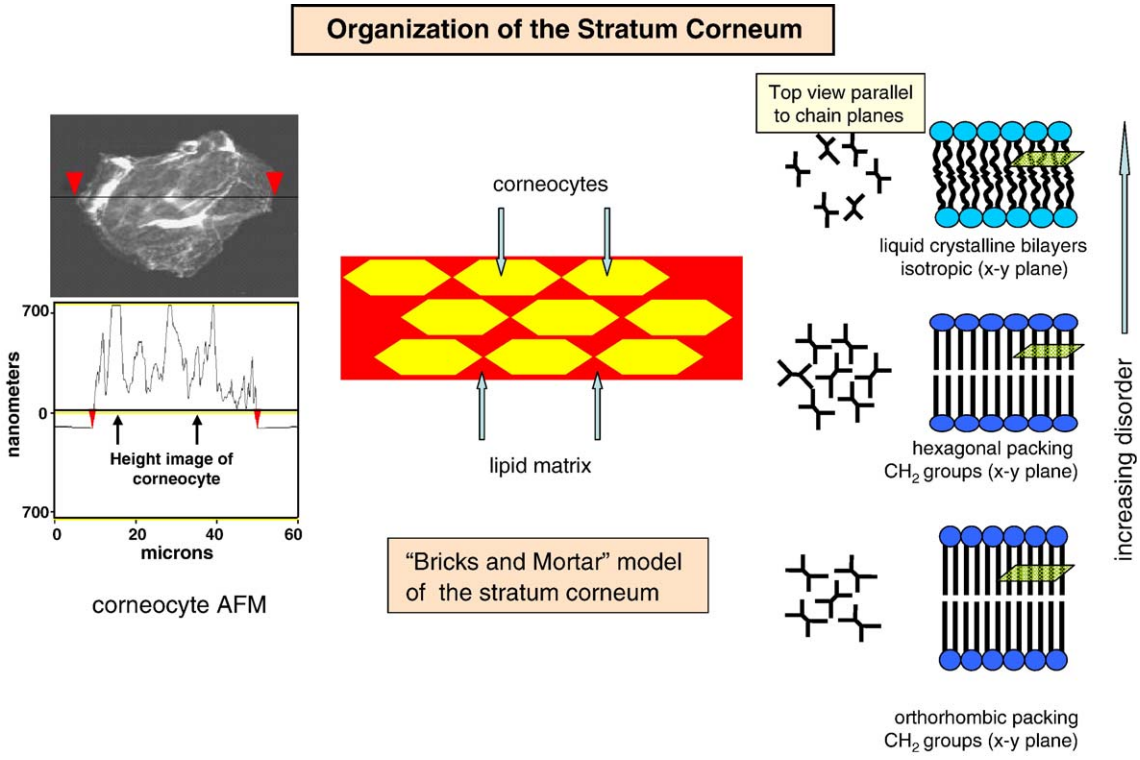

Fig. 2. "Bricks and mortar" model of stratum corneum organization. Left: an AFM image of a human corneocyte (top) isolated from ~1.5 μm underneath the skin surface with its height profile along the line drawn across the image shown at the bottom. The cell displays characteristic polygonal shape and size. Center: a cartoon of corneocyte distribution within the lipid matrix of the stratum corneum. Elongated corneocytes (thickness ~0.5–0.8 μm) overlie each other and together with the stacked bilayers of the lipid matrix provide a tortuous route for the permeation of exogenous substances. Right: a schematic of the conformationally ordered (bottom) and disordered (top) lipid phases thought to simultaneously exist in the lipid matrix of the stratum corneum.

more elaborated model due to Forslind [6], termed the "Domain Mosaic Model," considers the supramolecular organization of the lipid matrix. Most of the lipids are suggested to be segregated into ordered orthorhomic and hexagonally packed lipid domains (depicted in the right hand panel of the figure) bordered by "grain boundaries" where some shorter chain, conformationally disordered (liquid crystalline) lipids are presumed to be located. These latter regions are suggested to represent areas through which hydrophobic species may diffuse. Furthermore, in these regions, structural transformations of the lipid induced by permeation enhancers may occur without alterations in the structures of the more ordered phases.

Finally, in addition to the corneocytes and lipid lamellae, water plays a key role in maintaining stratum corneum barrier integrity [7]. Environmental humidity affects the activities of enzymes involved in the desquamation process as well as influences lipid phase behavior [8].

2.5.3. Vibrational spectroscopy of lipids

Four decades of seminal studies by amongst others, Snyder and Zerbi and their respective co-workers have produced a detailed understanding of relationships between alkane phases and their vibrational spectra. For over 30 years, IR and Raman investigations of lipid assemblies in many physical states from intact cells to Langmuir films have been reported from many laboratories in addition to our own (e.g. Levin (NIH), Blume (Germany), Mantsch (Ottawa), Pézolet (Quebec City), Peticolas (Oregon), Wartewig (Halle), Dluhy (Georgia)). Many biologically important spectra–structure correlations have been developed using the alkane spectra as a guide. Those features of the vibrational spectrum which are currently potentially useful for studies of skin lipids are summarized in Table 1.

As noted in the table, several chain modes are sensitive to various aspects of molecular conformation and interaction. The methylene stretching frequencies qualitatively monitor both lipid conformational order and acyl chain packing. The sensitivity to conformational order (*trans-gauche* isomerization in the chains) is well known. However, although the sensitivity of these modes to acyl chain packing is not as widely utilized, this aspect nevertheless is important for studies of ordered domain formation and solid–solid phase transitions that occur in the ceramide constituents of the SC [9,10]. For the symmetric CH_2 stretching frequency (ν_{sym} CH_2) which ranges from 2847 to 2855 cm^{-1}, the band position distinguishes packing from conformational effects. Packing geometry alterations (usually arising from solid–solid phase transitions) are inferred if cooperative changes in ν_{sym} CH_2 appear below ~2850 cm^{-1}, while the introduction of *gauche* rotamers into the acyl chains causes ν_{sym} CH_2 to exceed this value. As this mode is both intense and not overlapped by other vibrational modes in the IR spectrum of skin, we have found it useful for conformational studies. In addition, if the acyl chains of an exogenous liposome are deuterated, the CD_2 stretching modes appear in a spectral region (2080–2210 cm^{-1}) free from interference from other components. The conformational state of the exogenous species can then be specifically monitored in addition to the endogenous CH_2 stretching modes.

Table 1
Lipid vibrational frequencies for structural and imaging applications

Vibrational mode	Frequency range (cm^{-1})	Sensitivity
CH_2 symmetric stretch	2847–2855	The frequencies qualitatively monitor chain conformational order and packing.
CH_2 asymmetric stretch	2915–2924	The asymmetric stretching modes are less sensitive to packing changes.
CD_2 symmetric stretch	2088–2097	
CD_2 asymmetric stretch	2193–2198	
CH_2 scissoring	1462,1473	The splitting reveals the presence of orthorhombic perpendicular packing. The band contour defines the domain size distribution function.
	1468	Usually hexagonal chain packing.
	1473	Triclinic chain packing.
CD_2 scissoring	1086,1094	The splitting reveals the presence of an orthorhombic perpendicular packing for perdeuterated lipid chains.
	1089	Hexagonal packing for perdeuterated lipid chains.
CH_2 rocking	720,730	The splitting reveals the presence of orthorhombic perpendicular packing.

While the methylene stretching modes provide a qualitative description of intrachain conformational order and packing characteristics, the scissoring modes (1462–1473 cm^{-1} for proteated species, 1086–1094 cm^{-1} for deuterated species) provide a means for directly detecting orthorhombic phases and microaggregation in ordered lipid phases [11,12]. Similar considerations are pertinent for the rocking modes between 720 and 730 cm^{-1}.

2.6. IR microspectroscopy of conformational order in skin lipids

2.6.1. IR spectroscopy of isolated stratum corneum

The sensitivity of several IR parameters to structural transitions in isolated SC is demonstrated in Figs. 3A–C. In Fig. 3A, the CH_2 symmetric stretching frequency increases cooperatively over the temperature range ~80–90 °C, thereby reflecting the major order–disorder transition from hexagonally packed to disordered chains in the SC lipids. This transition is analogous to the widely studied gel→liquid crystal phase transition in phospholipids. In addition, a second transition accompanied by a small frequency increase of ~0.5 cm^{-1} is observed between about 20–40 °C, and is attributed to a solid–solid (orthorhombic→hexagonal) phase interconversion. Similar effects have been observed by Ongpipattanakul et al. [13].

As noted above, the CH_2 scissoring modes are very sensitive to solid–solid phase transitions. In Fig. 3B, the occurrence of orthorhombic phases is revealed by the splitting of the

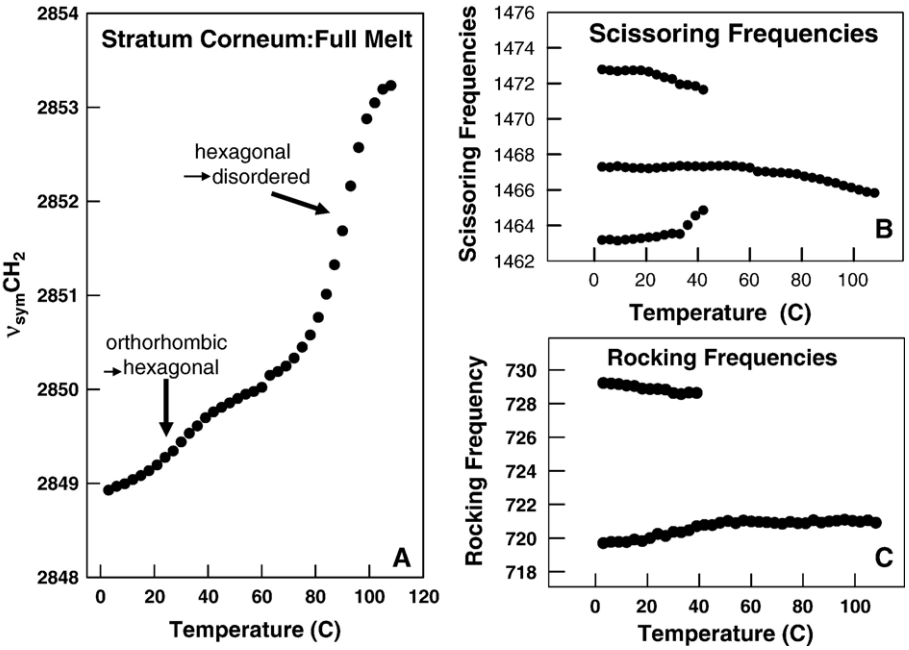

Fig. 3. Temperature-induced changes in IR spectral parameters evaluating lipid acyl chain conformational order and packing in isolated human stratum corneum. (A) CH_2 symmetric stretching frequency response to temperature displaying two transitions as marked, and (B) CH_2 scissoring frequencies and (C) CH_2 rocking frequencies as a function of temperature accentuating the solid–solid phase transition at ~40 °C.

scissoring modes to produce a doublet with components at ~1473, 1463 cm^{-1}. As the temperature increases, the two outer frequency branches approach each other to the point where the splitting collapses at the orthorhombic→hexagonal transition. This temperature coincides with the transition detected in the CH_2 stretching vibration. The central branch of the figure, at temperatures <40 °C, represents lipids not present in orthorhombic phases. This branch decreases slightly in frequency as the temperature is increased. Similar effects are observed for the CH_2 rocking modes (Fig. 3C). In this instance, no central component is observed since the rocking frequency of hexagonal lipid phases appears close to 720 cm^{-1}.

2.6.2. Attenuated Total Reflectance (ATR) IR of stratum corneum: introduction of Z-dimension spatial resolution

Horizontal ATR (HATR) IR spectroscopy has been used to collect high quality IR spectra of full thickness skin normally with the SC aspect of the skin placed against the ATR crystal. The acquired spectra are from the outer surface (~2 μm) of the sample. A significant advantage to the HATR technique is that the skin sample requires no preparation thereby minimizing possible damage to the sample. A single spectrum is collected, which although highly resolved in the *Z*-dimension, has no *X*–*Y* spatial resolution and is in essence the average spectrum across the area sampled. When utilized as just described, HATR IR spectroscopy of skin, both ex vivo and in vivo, is a very useful technique for measuring deposition of materials on the surface of skin or delivered into the SC [14,15]. In addition, HATR IR spectroscopy can provide significant and otherwise unavailable depth-dependent IR spectral information when combined with a simple physical sampling technique such as sequential tape stripping. This technique uses standard adhesive ("scotch"™) tape to remove a layer of SC with each sequentially applied piece of tape, in effect leaving skin with a slightly thinner (~0.5 μm) SC after each tape strip is removed. Sequential tape stripping is widely applied in analytical studies of SC, in which the tape is extracted with organic solvents and chromatographic techniques are used to provide quantitative data on specific endogenous or exogenous molecules [16,17].

The combination of sequential SC tape stripping with HATR IR spectroscopy of skin provides a method for acquiring *Z*-resolved spectra of the SC if the stripped skin is placed SC side on the HATR crystal after each tape strip is removed. Thus while the measurement provides a sampling of ~2 μm of SC, the sequential removal of the outermost SC layer with tape provides a method for "stepping" deeper into the tissue. Sequential *Z*-resolved IR spectra of SC can be acquired right through the SC as first demonstrated by Potts and Guy [18]. A series of HATR IR spectra, from our laboratories, of sequentially tape stripped porcine skin are shown in Figs. 4A and B, focusing on the 2800–3100 and 1575–1700 cm^{-1} spectral regions, respectively. Each spectrum was acquired after two tape strips were applied and removed from the SC; therefore each is approximately 1 μm deeper into the SC. In the expanded panel of the C–H stretching region (Fig. 4A), the presence of a band at ~3010 cm^{-1} (arising from =C–H stretch) in the first few spectra reveals that the lipid composition contains significant numbers of unsaturated hydrocarbon chains. Such chains are not present in significant amounts in the SC and reveal the presence of other lipids, either from sebum and/or environmental contamination on the skin surface. The spectra in Fig. 4B show clearly that the corresponding spectra contain esters (~1740 cm^{-1}) indicating that the unsaturated lipids are triglycerides or phospholipids,

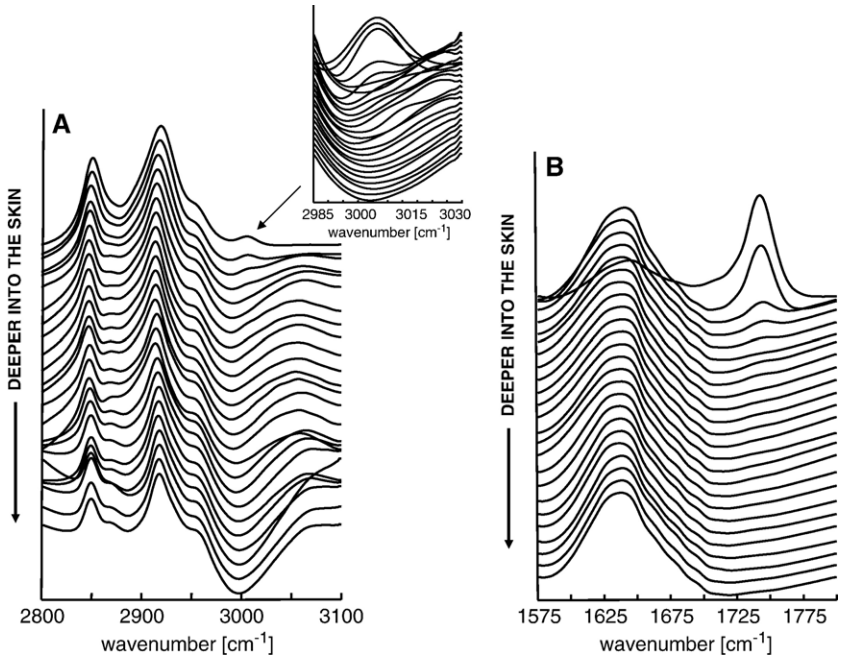

Fig. 4. HATR IR spectra of pigskin upon sequential tape stripping from the skin surface to a depth of ~25 μm (top to bottom, respectively) in steps of ~1 micron (two tape strips were drawn between each spectrum). (A) The 2800–3100 cm^{-1} region displaying the symmetric and asymmetric CH_2 stretching modes at ~2850 and 2920 cm^{-1}, respectively. (inset) Enlargement of the 2985–3030 cm^{-1} region to emphasize the =C–H stretching band at ~3010 cm^{-1} in the top few spectra. (B) The 1575–1800 cm^{-1} region displaying an ester carbonyl stretching band at ~1740 cm^{-1} in the top few spectra corresponding to sebum or contamination on the skin surface and the amide I mode at ~1635 cm^{-1} due to the ceramide and protein constituents.

neither of which are endogenous to the SC barrier lipid matrix. Lipid structural information is also available from these spectra. A change in SC lipid conformation with depth (*Z*-resolution) is revealed by the changing frequency of the symmetric CH_2 peak at ~2850 cm^{-1}, visible in the stacked spectra of Fig. 5A but more obvious in the plot of $\nu_{sym}CH_2$ against *Z*-depth in Fig. 5B. The HATR IR data in Figs. 4 and 5 thus provide a direct link between molecular composition, conformational order and physiological function. When unsaturated lipids are present in the outer surface (above the functional SC) the overall lipid conformation is more disordered, however, within the functional SC the lipids are saturated and highly conformationally ordered. As such, SC lipids are able to provide the critical water-barrier function required of the SC lipid matrix. In addition, these *Z*-resolved HATR spectra illustrate that once the SC has been completely removed (or crossed) the lipids of the epidermis are again more disordered/fluid as expected of most biological membranes. Thus, although it is ultimately a destructive sampling method, the use of HATR IR spectroscopy and tape stripping is a powerful method for providing *Z*-resolved IR spectra of skin with all their inherent composition and conformational information.

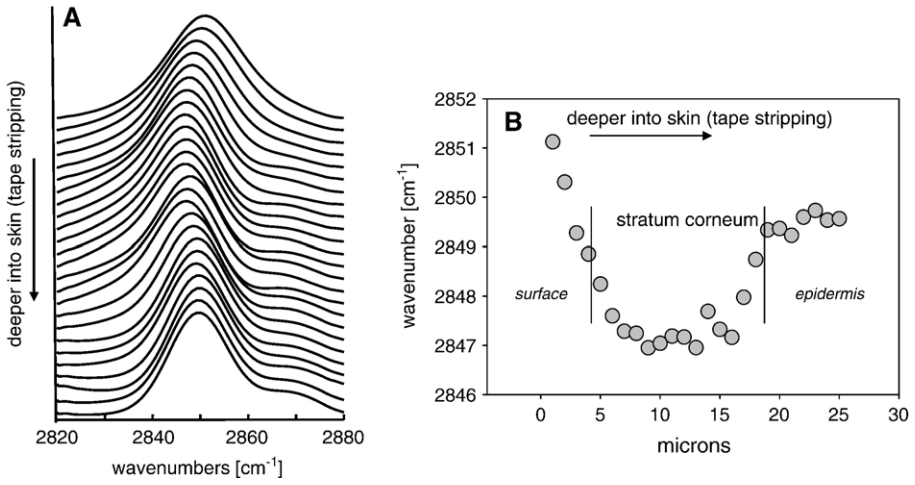

Fig. 5. (A) HATR IR spectral region 2820–2880 cm^{-1} of tape stripped pigskin (see Fig. 4, caption) revealing frequency shifts in the symmetric CH_2 stretching mode. (B) Frequency of the symmetric CH_2 stretching mode plotted as a function of depth in the skin.

2.6.3. IR microscopic imaging of skin: addition of X and Y resolution

The ability to monitor and image spatially resolved molecular structure information from skin is depicted in Fig. 6. The sample is a section of pigskin microtomed perpendicular to the surface to a thickness of ~5 μm, comprising an area of ~150×200 μm which is sampled by ~770 IR spectra.

Skin regions are labeled in the visual micrograph (Fig. 6A). Although, as noted previously, the diffraction limit and the IR detector pixel size impose constraints as to the number of IR spectra that may be acquired from the SC in a single line perpendicular to the surface, spectra characteristic of each skin region may nevertheless be isolated. For example, typical spectra of the C–H stretching region from the SC, the epidermis, and the dermis are depicted in Fig. 6C. In addition to the lipid (ceramide and fatty acid) CH_2 stretching vibrations at ~2850 and 2920 cm^{-1} which dominate the SC C–H stretching region, the presence of progressively increasing levels of protein in the epidermis and dermis is monitored by the appearance of the symmetric and asymmetric CH_3 stretching modes near 2872 and 2955 cm^{-1}, respectively.

An image of the spatial variation of lipid conformational order is presented in Fig. 6B. Significant variation in chain conformational order is observed in progressing from the stratum corneum where the chains are highly ordered (ν_{sym} CH_2 ~2849–2850 cm^{-1}) to the dermis, where substantial disorder occurs (ν_{sym} CH_2 ~2853–2854 cm^{-1}). We note that the frequency in the most ordered regions is in excellent agreement with the isolated SC data in Fig. 3 although ~2 cm^{-1} higher than the lowest values observed in the ATR measurements from a tape stripped sample corresponding to a depth of about 7 μm (compare Fig. 6B with Fig. 5B). The quantitative origin of this shift is uncertain but may arise in part from frequency decreases known to occur when ATR measurements are compared with transmission IR [19].

2.6.4. Lipid conformational changes caused by permeation of liposomes

With the ability to image lipid conformational order changes proven, we illustrate the applicability of this approach to an issue of current interest in skin pharmaceutics. Liposome formulations have been widely investigated and in some cases used as transdermal drug delivery vehicles [20]. Structural perturbations resulting from the interaction of these formulations with skin cannot easily be directly studied except by vibrational microscopy. The object of this experiment is to elucidate molecular structure changes induced in both the endogenous lipids of the SC and in the exogenous lipids of the liposomes incorporated into the SC. Two simple phospholipid vesicle preparations for this purpose, acyl chain perdeuterated 1,2-dimyristoylphosphatidylcholine (DMPC-d_{54}) and 1-palmitoyl-d_{31}, 2-oleoylphosphatidylcholine (P-d_{31}OPC), were employed. Deuteration of one or both acyl chains provides a spectroscopic "handle" convenient to monitor the conformational state of the exogenous lipid.

Figs. 7A–C depict the results of a study in which P-d_{31}OPC was permitted to permeate into hairless pig skin, a standard dermatological model. The visible micrograph (Fig. 7A) clearly depicts the SC, the epidermis, and dermis as marked. In addition, a thin layer of residual surface liposomes may be seen, albeit at poor contrast, above the SC. Fifteen spectra taken along a single *Z* line (extending perpendicular to the surface) into the stratum corneum are depicted in Figs. 7B and C. The direction of the arrows in Figs. 7B and C, corresponds to the arrow direction in Fig. 7A. Spectral quality is excellent. The first (bottom) spectrum is outside the skin region. The succeeding ten spectra exhibit C–D stretching vibrations and reflect the presence of the POPC-d_{31}. The skin begins to contribute significantly to the IR data in about the 7th or 8th spectrum, as noted from the appearance of the keratin Amide I and II vibrations.

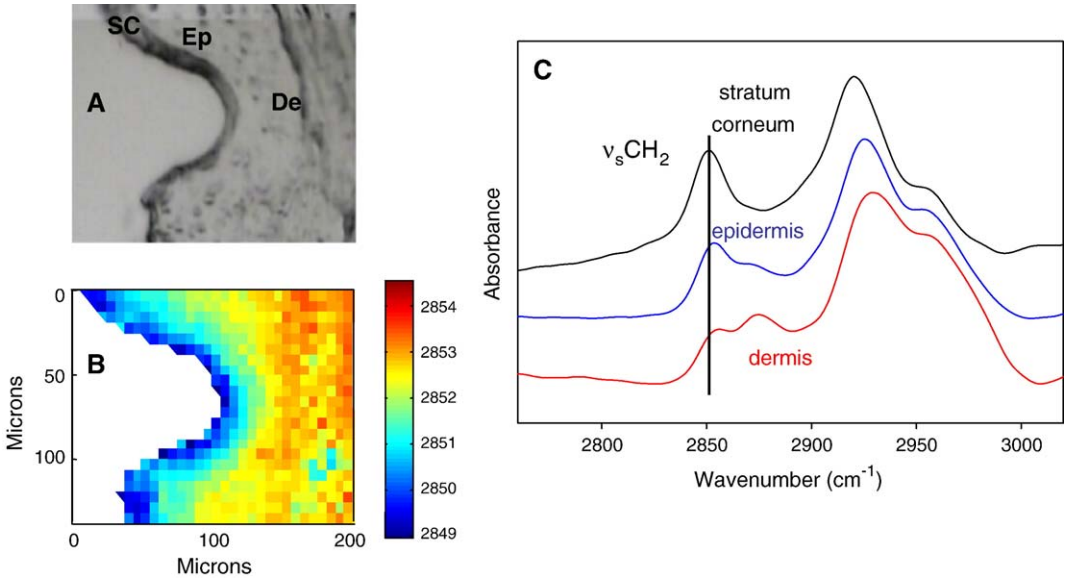

Fig. 6. (A) An optical micrograph of a 5-μm thick unstained pigskin section from which (B) an IR image of the symmetric CH_2 stretching frequency was obtained. (C) Single pixel IR spectra of the CH stretching region selected from regions in skin as labeled. The absorbance scales of the three spectra differ.

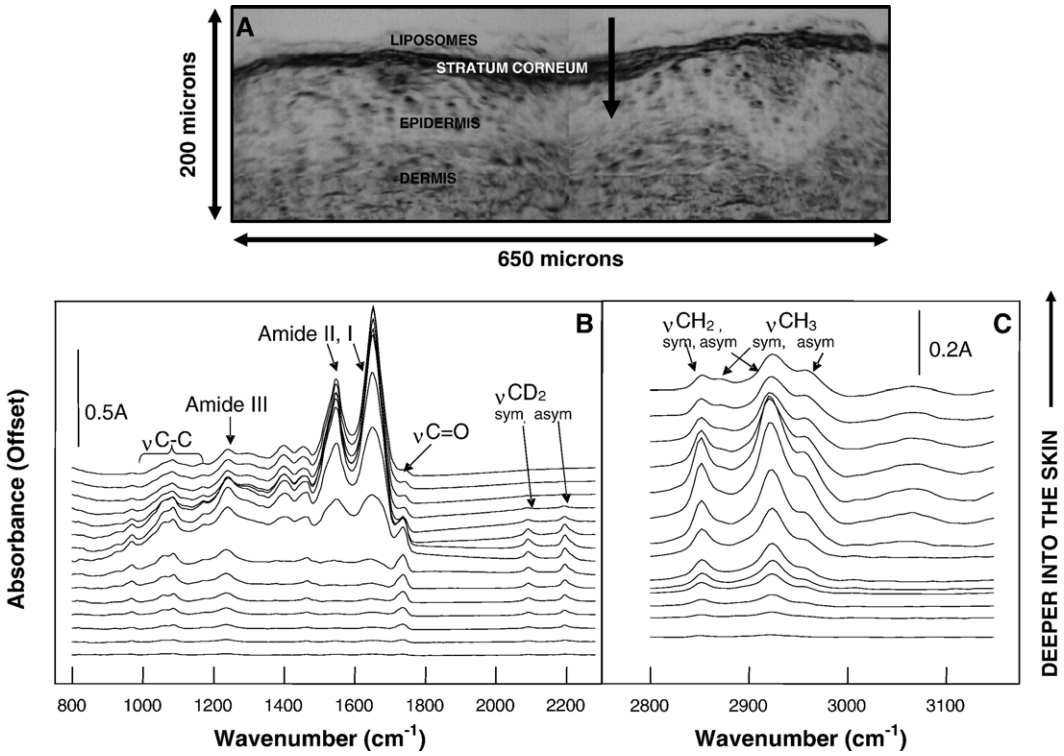

Fig. 7. (A) A visible image of a 5-μm-thick unstained pigskin section after incubation with P-d_{31}OPC liposomes at room temperature for 2.5 h. (B) The 800–2230 cm^{-1} region and (C) the CH stretching region for spectra selected from an IR image acquired of the skin section along the arrow drawn in (A) from outside the skin to within the viable epidermis. Spectra are stacked from bottom to top, respectively. The thick arrows in panels B and C correspond to spectra taken along the arrow in panel A. The 15 spectra shown in B and C were collected over a region corresponding to the length of the arrow (corresponding to ~90 μm) in panel A. The pixel size was 6.25 μm.

Permeation of liposomes along the single *Z* line (extending perpendicular to the surface in Fig. 7A) into the stratum corneum is depicted quantitatively in Fig. 8A. The extent of permeation is monitored by comparison of the intensity of the CD_2 stretching vibration with the Amide II mode (~1550 cm^{-1}) of skin proteins. The former provides a measure of relative liposome concentration while the latter provides a measure of the location of the liposome–skin interface (at the horizontal scale position of 45 μm). As is evident from the figure, the P-d_{31}OPC permeates ~40–50 μm into the skin.

Of interest for current purposes is our ability to detect conformational differences between the permeated P-d_{31}OPC and that remaining in surface liposomes. We used factor analysis for this purpose. Loadings from three factors extracted from the CD_2 stretching region are depicted in Fig. 8B. Score plots of these factors are presented in Figs. 8C–E. The score plot in Fig. 8C (ν_{sym} CD_2=2091.7 cm^{-1}) arises primarily from vesicles localized on the skin surface in the residual reservoir seen in the micrograph (Fig. 7A), whereas the score plot in 8D (ν_{sym} CD_2=2091.5 cm^{-1}), arises from liposomes permeated into the SC. Finally, the score plot in Fig. 8E depicts a third class of lipid (ν_{sym} CD_2=2090.9 cm^{-1}) that has apparently permeated through the SC into the epidermis. The power of factor analysis is revealed by a combination of these score plots with the conformational information that may be extracted from examination of the loadings in Fig. 8B. Although the loadings presented in the figure appear quite similar, the high signal-to-noise ratios in the original spectra (as well as multiple repeat experiments performed) engender confidence that the slight differences between them as noted above are meaningful.

Our interpretation of these frequency alterations is that the permeated P-d_{31}OPC deuteriopalmitate chains (Fig. 8E) are conformationally more ordered than those remaining on the surface. Considering the highly ordered nature of the SC chains, it is further suggested that, upon permeation, the deuteriopalmitate chains mix with the SC lipids producing more ordered P-d_{31}OPC. This interpretation is consistent with a model suggesting disruption of some exogenous vesicles upon permeation. This result is an important consideration for drug delivery issues [21].

The second issue of interest is evaluation of conformational alterations within the native SC lipids induced by the exogenous liposomes. To address this problem, exogenous perdeuterated DMPC-d_{54} vesicles were utilized, since they lack CH_2 stretching vibrations that would otherwise interfere with the same modes in the endogenous SC. To provide a "thicker" SC for IR spectroscopic sampling, the SC in each sample was swollen to 40–50 μm. A visible micrograph from a section of swollen pigskin lacking added exogenous vesicles is shown in Fig. 9A, along with an image of the CH_2 stretching frequencies generated from the IR spectra (Fig. 9B), and a histogram of these values (Fig. 9C). Regions of the image on the outside of the skin and in the dermis have been masked. The image (which includes both the SC and the epidermis) in Fig. 9A depicts

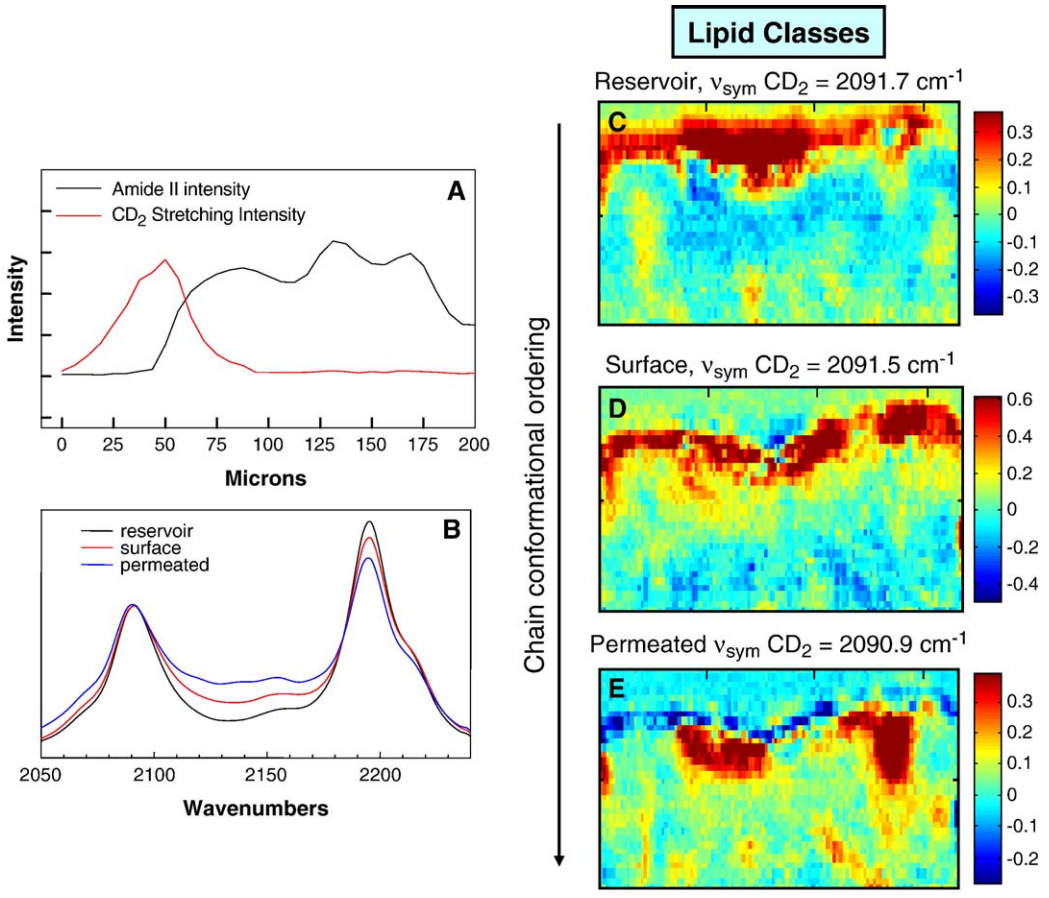

Fig. 8. (A) The intensity of the symmetric CD_2 stretching mode after pigskin incubation with P-d_{31}OPC vesicles (red) and the intensity of the native skin amide II band (black) as a function of position in the skin sample shown in Fig. 7A along the arrow and deeper into the dermis. (B) The results of factor analysis in the CD stretching region for the pigskin section. Three factor loadings are shown with small frequency shifts just discernable in the symmetric and asymmetric CD_2 stretching modes. Peak picking the second derivatives of the loadings illuminates the frequency shift and the position of the symmetric CD_2 stretching band is shown along with images of each factor's score in (C–E). A decrease in the symmetric CD_2 stretching frequency is revealed as the liposomes permeate the skin.

significant structural differences between the outermost layer (mostly the SC) and the deeper layer of the epidermis. These structural differences are clearly reflected in the bimodal histogram. The lower frequency peak in the histogram at ~2851.5 cm^{-1} is clearly derived from the SC layer. The wavenumber value is higher than that observed in unswollen skin (2849–2850 cm^{-1}, see Fig. 6), and probably reflects chain disordering events associated with the swelling process. A thin layer of more highly ordered lipids may be detected at the SC surface. The second peak in the bimodal histogram at ~2853.1 cm^{-1} reflects the conformational state of lipid in the deeper epidermal layers. This frequency is fairly concordant with those in the unswollen sample (Fig. 6B).

Addition of DMPC-d_{54} liposomes induces significant increases in native SC chain conformational disorder. The data are shown in Fig. 9D where the optical image is presented and in Figs. 9E and F where an image and histogram of the $\nu_{sym}CH_2$ frequencies are presented, respectively. The histogram of $\nu_{sym}CH_2$ reveals some significant alterations compared to the untreated section. Although the histogram is still bimodal, the nature of the distribution function is altered from Fig. 6C. The low frequency peak in the distribution is increased in position by about 0.5 cm^{-1}; more important, as is evident from both the image and histogram, a significant "filling-in" of histogram values near 2852.5 cm^{-1} has occurred. This alteration evidently arises from liposome-induced disordering of some of the SC lipids. Finally, the higher frequency peak in the histogram (Fig. 9C) at 2853.0 cm^{-1} is shifted to higher values in the liposome treated skin (Fig. 9F). The origin of this may be trivial in that in Fig. 9E, a greater proportion of dermis is sampled than in Fig. 9B. Overall, addition of DMPC-d_{54} liposomes significantly increases the average native SC lipid conformational disorder.

2.7. Preliminary applications to protein conformation in single cells

An additional novel application for vibrational microscopy and imaging is that the biophysical properties of the components of single cells may be determined. Sampling problems from anucleated single corneocytes in the SC are minimal. One issue of interest in dermatology and dermal delivery is the examination of the effects of solvents and other formulation emollients commonly used as permeation enhancers or to solubilize topical drugs, on major skin proteins such as keratin in its native cellular environment.

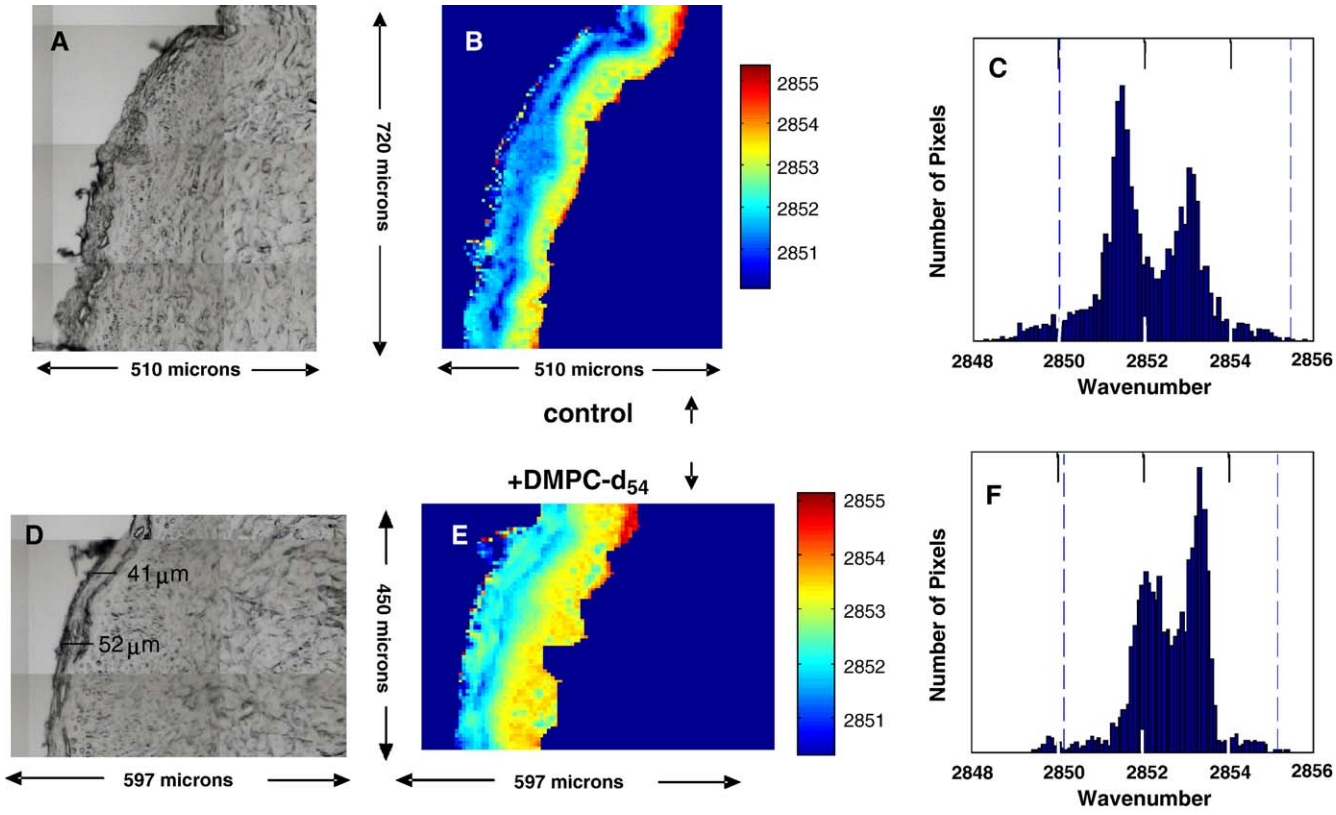

Fig. 9. This figure presents an IR evaluation of endogenous stratum corneum lipid acyl chain conformational order in the absence (top 3 panels) and presence (bottom 3 panels) of incubation with DMPC-d_{54} liposomes using pigskin where the stratum corneum has been swollen. (A and D) Visible micrographs of microtomed pigskin sections without and with liposome application, respectively. (B and E) Spatially masked (stratum corneum and underlying epidermal regions highlighted) IR images of the symmetric CH_2 stretching frequency over the range shown between the dashed lines in the respective histograms of frequency distribution shown in (C and F). Lower frequencies are clearly evident in the stratum corneum of the untreated sample (B compared to E).

To begin to address this issue, corneocytes were isolated from skin and treated with dimethyl sulfoxide (DMSO). The IR results are shown in Fig. 10. In trace "a", the spectrum of a single corneocyte before treatment with DMSO is shown. An intense Amide I feature arising from the helical keratin secondary structure is shown. There are startling changes noted upon treatment of the corneocyte with DMSO. Addition of DMSO leads to the formation of an intense new feature (trace "b") near 1620 cm^{-1}, revealing the formation of extensive antiparallel β-sheet structure in the protein. Also interesting is the observation (trace "c") that rehydration of the corneocyte mostly reverses the effect of the DMSO treatment, leading to the disappearance of the Amide I band characteristic of sheet structure and the reformation of the 1655 cm^{-1} band characteristic of the helical structure. Equivalent results were obtained from the Raman measurements (not shown). On going studies indicate that the reversibility of these structural changes are solvent dependent. It is anticipated that IR imaging will provide some insight into the spatial distribution of these structural changes in single corneocytes.

3. Concluding comments

The current studies clearly demonstrate that the inherent ability of vibrational microscopic methods to monitor conformational changes in lipids and proteins may be extended to sampling regimes of biological and perhaps clinical interest. It is possible to conceive of a variety of issues which could be profitably studied by vibrational microscopy. Obviously the permeation of exogenous agents and the evaluation of structural alterations in skin constituents, including single cells, during

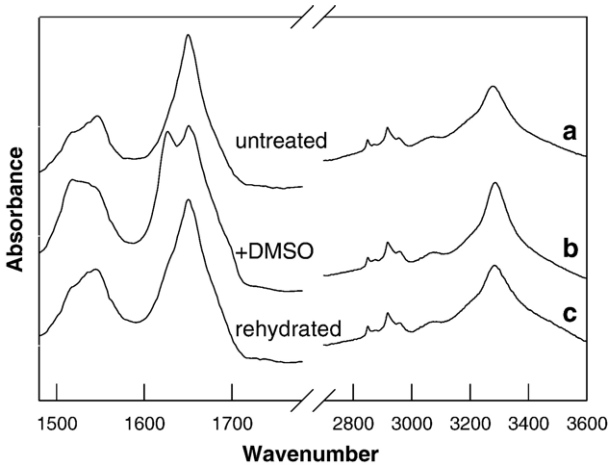

Fig. 10. IR spectra of an isolated human corneocyte (a) before and (b) after treatment with DMSO. Large changes are observed in the amide I and II band contours (1480–1700 cm^{-1} region), whereas the high wavenumber region, in particular the methyl and methylene stretching bands (2800–3000 cm^{-1}) show little change. A spectrum acquired after rehydration of the corneocyte (c) shows that the DMSO-induced changes are reversible.

permeation are all feasible and have been demonstrated in this article and in our published work.

Acknowledgements

This work was supported by PHS Grant GM-29864 to RM. We thank two current graduate students, Chunhong Xiao and Guojin Zhang, and a former student, Hui-Chen Chen, for their important contributions to the work described in this article. Their excellent contributions have been formally recognized in the published work from this laboratory.

References

[1] G. Zhang, D.J. Moore, R. Mendelsohn, C.R. Flach, Vibrational microspectroscopy and imaging of molecular composition and structure during human corneocyte maturation, J. Invest. Dermatol. 126 (2006) 1088–1094.

[2] C. Xiao, D.J. Moore, C.R. Flach, R. Mendelsohn, Permeation of dimyristoylphosphatidylcholine into skin—Structural and spatial information from IR and Raman microscopic imaging, Vibr. Spectrosc. 38 (2005) 151–158.

[3] C. Xiao, D.J. Moore, M.E. Rerek, C.R. Flach, R. Mendelsohn, Feasibility of tracking phospholipid permeation into skin using Infrared and Raman microscopic imaging, J. Invest. Dermatol. 124 (2005) 622–632.

[4] C. Xiao, C.R. Flach, C. Marcott, R. Mendelsohn, Uncertainties in depth determination and comparison of multivariate with univariate analysis in a laminated polymer and skin, Appl. Spectrosc. 58 (2004) 382–389.

[5] R. Mendelsohn, H.-C. Chen, M.E. Rerek, D.J. Moore, Infrared microscopic imaging maps the spatial distribution of exogenous molecules in skin, J. Biomed. Opt. 8 (2003) 185–190.

[6] B. Forslind, A domain mosaic model of the skin barrier, Acta Derm. Venerol. 74 (1994) 1–6.

[7] I.H. Blank, J. Moloney III, A.G. Emslie, I. Simon, C. Apt, The diffusion of water across the stratum corneum as a function of its water content, J. Invest. Dermatol. 82 (1984) 188–194.

[8] A.V. Rawlings, I.R. Scott, C.R. Harding, P.A. Bowser, Stratum corneum moisturization at the molecular level, J. Invest. Dermatol. 103 (1994) 731–740.

[9] M. Lafleur, Phase behaviour of model stratum corneum lipid mixtures: an infrared spectroscopy investigation, Can. J. Chem. 76 (1998) 1501–1511.

[10] D.J. Moore, R.G. Snyder, M.E. Rerek, R. Mendelsohn, Kinetics of membrane raft formation: fatty acid domains in stratum corneum lipid models, J. Phys. Chem. 110 (2006) 2378–2386.

[11] R.G. Snyder, V.J.P. Srivastovoy, D.A. Cates, H.L. Strauss, J.W. White, D.L. Dorset, Hydrogen/deuterium isotope effects on microphase separation in unstable crystalline mixtures of binary n-alkanes, J. Phys. Chem. 98 (1994) 674–684.

[12] R.G. Snyder, H.L. Strauss, D.A. Cates, Detection and measurement of microaggregation in binary mixtures of esters and of phospholipid dispersions, J. Phys. Chem. 99 (1995) 8432–8439.

[13] B. Ongpipattanakul, M.L. Francoeur, R.O. Potts, Polymorphism in stratum corneum lipids, Biochim. Biophys. Acta 1190 (1994) 115–122.

[14] A. Naik, L.A.R.M. Pechtold, R.O. Potts, R.H. Guy, Mechanism of oleic-induced skin penetration enhancement in vivo in humans, J. Control. Release 37 (1995) 299–306.

[15] V.H.W. Mak, R.O. Potts, R.H. Guy, Percutaneous penetration enhancement in vivo measured by attenuated total reflectance infrared spectroscopy, Pharm. Res. 7 (1990) 835–841.

[16] G. Potard, C. Laugel, H. Schaefer, J.-P. Marty, The stripping technique: in vitro absorption and penetration of five UV filters on excised fresh human skin, Skin Pharmacol. Appl. Skin Physiol. 13 (2000) 336–344.

[17] U. Lindemann, H.-J. Weigmann, H. Schaefer, W. Sterry, J. Lademann, Evaluation of the pseudo-absorption method to quantify human stratum corneum removed by tape stripping using protein absorption, Skin Pharmacol. Appl. Skin Physiol. 16 (2002) 228–236.

[18] D. Bommannan, R.O. Potts, R.H. Guy, Examination of stratum corneum barrier function in vivo by infrared spectroscopy, J. Invest. Dermatol. 95 (1990) 403–408.

[19] M.W. Urban, Attenuated Total Reflectance Spectroscopy of Polymers: Theory and Practice, Polymer Surfaces and Interfaces Series, American Chemical Society, Washington, DC0-8412-3348-9, 1996.

[20] G. Cevc, Lipid vesicles and other colloids as drug carriers on the skin, Adv. Drug Deliv. Rev. 56 (2004) 675–711.

[21] P.L. Honeywell-Nguyen, A.M. de Graaff, H.W.W. Groenink, J.A. Bouwstra, The in vivo and in vitro interactions of elastic and rigid vesicles with human skin, Biochim. Biophys. Acta 1573 (2002) 130–140.